

# Replicating a Model of Viral Spread in Bronchial Epithelium

Alexander Southern, Emma Alexandrov, & Pedro dal Castel

April 2024

## Abstract

We simplify and replicate the model of viral spread and innate immune response in bronchial epithelial cells reported in [1], which supports digital versions of “viral plaque assay” experiments performed *in vitro*. Using this model is less expensive than carrying out these experiments, and it may be more informative in certain cases. The model consists of a mathematical representation of viral replication and interferon-mediated immunity through ordinary differential equations (ODEs) as well as a computational representation of cell health through a probabilistic finite state machine. The model is implemented with CompuCell3d [2] and is designed to be immediately accessible by wet-lab researchers familiar with viral plaque assay methods. Here, we review the phenomena of interest, explain the model and its implementation, review changes made to the model in the interest of computational efficiency, and report the successful replication of four figures from the original paper.

## 1 Biological Background

In an effort to track the progress of viral infections in different types of tissues and to explore potential treatments, wet lab researchers perform experiments known as “viral plaque assays” in which a sheet, or “monolayer”, of cells is grown and then exposed to a virus of interest, typically in low concentrations. Infected cells burst, releasing viral particles, or virions, which infect adjacent cells, and as soon as two days after the application of the virus, regions of dead cells, or “plaques,” become visible to the unaided eye. Special care is taken to ensure that the virus spreads only to cells adjacent to sites of viral release, rather than through the flow of extracellular fluids [3].

Growing and maintaining the cell cultures required for viral plaque assays can be expensive,

and working with human viruses may present risk to researchers. These challenges prompt interest in the use of computer simulations of viral infection, which are cheaper and safer than wet experimentation.

One such simulation, designed by Aponte-Serrano et al., aims to capture the spread of infection by an RNA virus through bronchial epithelial cells of the lung, the innate immune responses of cells to the infection, and the interaction between the virus and these defenses and its effect on the outcome of the infection [1].

Innate immunity is one of the two facets of the immune response, the other being adaptive immunity. While adaptive immunity refers to processes involving the recognition of previously-encountered pathogens to the end of their destruction, innate immunity comprises a set of defenses that make cells generally resistant to viral replication, even up to the activation of proteins which destroy all single-stranded RNA and the cessation of all protein synthesis within infected cells [4]. Upon infection, a cell begins to produce and secrete molecules called interferons (IFNs), which trigger both interferon secretion and resistance to infection in neighboring cells. This interferon response serves the same function as an alarm sounded by a monkey upon spotting a jaguar. If cells are prepared to mount their defenses the moment virus reaches them, they can thwart viral replication and the their tissue can fend off infection.

Within an infected cell, cytosolic retinoic acid inducible gene I (RIG-I) and sensor proteins of the toll-like receptor (TLR) family detect the virus and ultimately trigger the production of interferons of types  $\alpha$  and  $\beta$ ; RIG-I senses viral RNA [5], while TLR-family proteins respond to a variety of so-called “Pathogen-Associated Molecular Patterns” known to the cell by way of evolutionary history [6].

IFN $\beta$ , in particular, prompts responses in both neighboring cells and the secreting cell itself [7]. When interferons  $\alpha$  and  $\beta$  are released and reach neighboring cells, they cause the addition of a phosphoryl group (“phosphorylation”) to the Signal Transducer and Activator of Transcription (STAT) protein by way of the Janus Kinase (JAK)-STAT pathway [8]. Cytokines bind to a special receptor embedded in the cell membrane, causing JAK to phosphorylate STAT [9]. Phosphorylated STAT, or STATP, lies at the head of a signalling pathway that culminates in the activation of Interferon-Stimulated Genes (ISGs), a group which includes genes whose products enact an anti-viral state within the cell, genes coding for RIG-I, and genes coding for the transcription factor

Interferon Regulatory Factor 7 (IRF7), which, if activated by phosphorylation, enables the transcription of genes for IFN $\alpha$  and intensifies the production and secretion of IFN $\beta$  should the virus succeed in entering the cell [7]. Contact with INF $\beta$  renders cells more likely to secrete IFNs  $\alpha$  and  $\beta$  upon the sensing of the virus by way of the induction of genes for RIG-I and IRF7. Thus, in uninfected cells, the sensing of IFN induces a “hyper-vigilant” state, but not the secretion of IFN, while in infected cells, the sensing of IFN triggers an intensification in IFN secretion, i.e., the amplification of the IFN signal (see pp. 7-9 of the original paper [1]).

Both influenza and SARS-CoV, and likely SARS-CoV, are adapted to thwart the innate immune response. These viruses produce a protein, “nonstructural protein 1”, which blocks the binding of viral RNA to RIG-I. It is present in the model reported in the original paper, though its activity is set to zero by default (see p.8 of the original paper, [1]).

## 2 Approach

Here, we give the technical details of the model by Aponte-Serrano et al., including the computational representation of cell health as well as mathematical representations of viral replication and intracellular signalling leading to the activation of innate immune defenses. To facilitate understanding, model variables will appear in green, constants will appear in red, and cell states will appear in blue. Values for all constants are reported in the table in Appendix A, which we reproduced from the original paper (see [1], pp. 11-2).

### 2.1 Computational model of cell health

Each cell has a state that captures its situation relative to the infection. In the original paper, discussion of this state-transition model takes place on pp. 6-7; the model is itself taken from another work cited in the paper [10].

A cell is either *uninfected* ( $U$ ), “eclipsed” ( $I_1$ ), meaning that it is releasing interferon to alert neighboring cells while it incubates the virus, *virus-releasing* ( $I_2$ ), meaning that it releases both virions and interferon, or *dead* ( $D$ ). Cells move through the states in this order: (1) uninfected, (2) eclipsed, (3) virus-releasing, (4) dead, or, in symbols,  $U \rightarrow I_1 \rightarrow I_2 \rightarrow D$ . Cells cannot skip steps, nor can they move backwards through the ordering; for example, it is impossible for a  $U$  cell to

enter the  $I_2$  state, or for a cell in state  $D$  to enter the  $U$  state. At each time step, each cell retains its state or progresses to the next one *independently of the other cells* with probabilities computed based on cell state, viral concentration, cell health, time, and constants (see [1], pp. 11-2, for the table of constants). That is, all cells respond to the presence of the virus by moving through the same states according to probabilities determined by the same equations, but the cells undergo this process independently of one another.

For a cell in the uninfected state, the probability of transition to the eclipsed state is given by Equation (1), where  $\beta$  is viral infectivity,  $V_e$  is viral concentration in the region surrounding the cell, and  $MCS$  is the time step of the simulation.

$$P(U \rightarrow I_1) = 1 - e^{-\beta[V_e]*MCS} \quad (1)$$

For a cell in the eclipsed state, the probability of transition to the virus-releasing state is given by Equation (2), where  $k$  is the eclipse phase delay, measured in hours.

$$P(I_1 \rightarrow I_2) = 1 - e^{-k*MCS} \quad (2)$$

For a cell in the virus-releasing state, the probability of transition to the dead state is given by Equation (3), where  $k_{61}$  is a constant,  $V$  is viral concentration within the cell,  $H$  is cell health, and  $MCS$  is the time step of the simulation.

$$P(I_2 \rightarrow D) = 1 - e^{-k_{61}[V][1-H]*MCS} \quad (3)$$

Generally, switching to the next state becomes more likely with time and, for the transitions from uninfected to eclipsed or from virus-releasing to dead, with higher concentrations of highly infective virus or declining cell health, respectively, as familiarity with the basic ideas of infection should lead us to expect. Note that in the original paper, these are Equations 1, 2, and 3, respectively.

## 2.2 Mathematical model of viral replication vs. innate immunity

The model includes a mathematical representation of interferon-mediated signalling within and between cells and of viral replication within cells. Concentrations of proteins known to be important

to this signalling are modeled explicitly; those proteins are interferon  $\alpha$  and  $\beta$  within the cell (combined and represented as **IFN**), the activated (phosphorylated) form of STAT, **STATP**, and **IRF7** and its activated (phosphorylated) form **IRF7P** (see [1], p. 8).

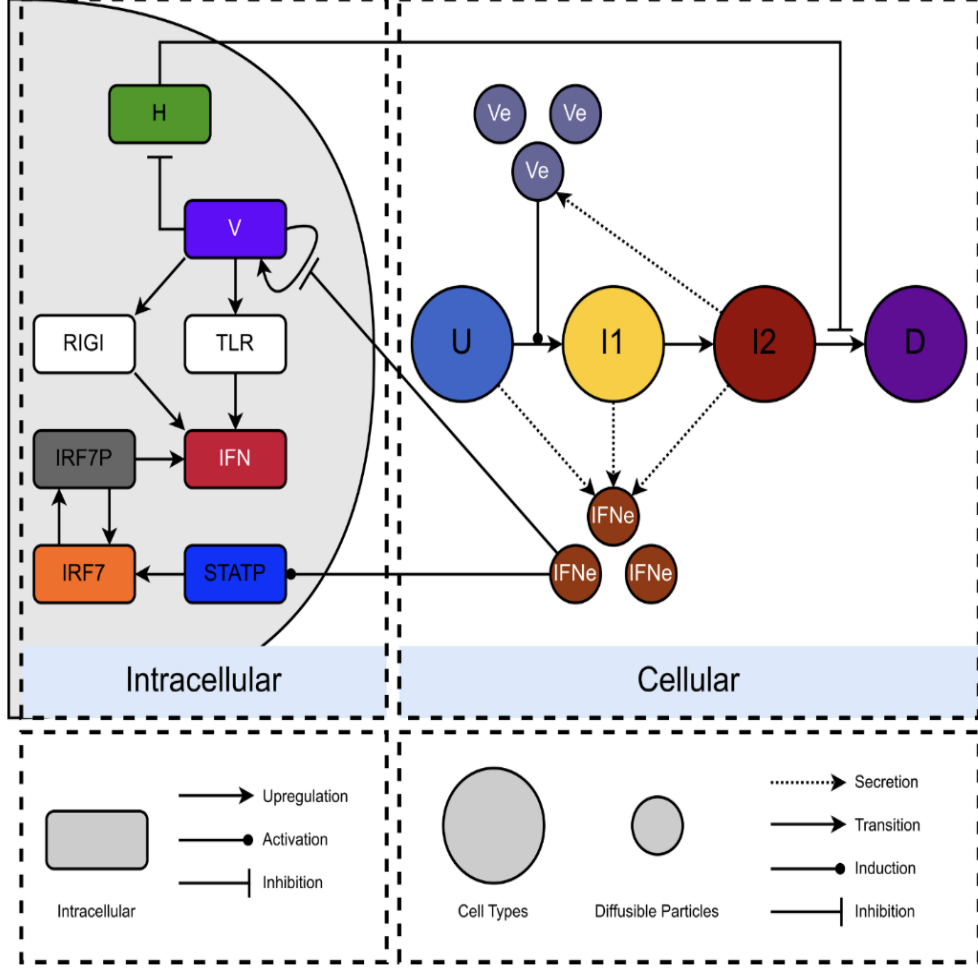


Figure 1: Diagram of signalling cascade within the cell (left) and cell health state transitions (right) reproduced from [1], where it appears as Figure 1. See the section ‘Computational model of cell health’ below for an explanation of the cell states.

Equation (4) gives the rate of change of interferon concentration *within a cell* (note that the rate of change of the interferon concentration *in the extracellular matrix* is given by Equation (10)):

$$\frac{d\text{IFN}}{dt} = H \left( k_{11} V + \frac{k_{12} V^n}{k_{13} + V^n} + k_{14} \text{IRF7P} \right) - k_{21} \text{IFN} \quad (4)$$

Interferon is the product of a cell in viral distress; this equation only applies to cells in states **I<sub>1</sub>** or **I<sub>2</sub>**. Interferon builds up in these cells to the extent that they are healthy (**H**), and the greater

the concentration of virions  $V$  and  $\text{IRF7P}$  within the cell, the faster the interferon concentration  $\text{IFN}$  increases. The interferon concentration within the cell decays over time, hence the subtraction of  $k_{21}\text{IFN}$ .

Equation (5) models the production of STATP within the cell as a function of cell health and contact with extracellular interferon:

$$\frac{d\text{STATP}}{dt} = \frac{k_{31}H * \text{IFN}_e}{k_{32} + k_{33}\text{IFN}_e} - \tau_3\text{STATP} \quad (5)$$

In general, the more extracellular interferon is sensed and the healthier the cell, the more STAT is activated within the cell. Like  $\text{IFN}$  above,  $\text{STATP}$  also decays, though at a different rate.

Equation (6) captures the production of IRF7, a transcription factor for  $\text{INF}\alpha$  (subsumed by  $\text{IFN}$  in the model):

$$\frac{d\text{IRF7}}{dt} = H(k_{41}\text{STATP} + k_{42}\text{IRF7P}) - \tau_4\text{IRF7} \quad (6)$$

To the extent that the cell is healthy, the greater the concentration of activated STAT (STATP) within the cell, the faster the cell will produce IRF7, reflecting that IRF7 is downstream of the phosphorylation of STAT in the signalling cascade. The activation of IRF7 also increases the rate of production of IRF7. Finally,  $\text{IRF7}$  decays.

Equation (7) gives the rate of change of IRF7P concentration, intended to reflect the activation of IRF7:

$$\frac{d\text{IRF7P}}{dt} = k_{51}H * \text{IRF7} - \tau_5\text{IRF7P} \quad (7)$$

As far as the cell is healthy, the more IRF7 there is within the cell, the faster IRF7P is produced. As with previous proteins, IRF7P concentration decays.

Equation (8) gives the rate of change of cell health:

$$\frac{dH}{dt} = -k_{61}H * V \quad (8)$$

Intuitively, cell health decays as a function of intracellular viral concentration.

Equation (9) gives the rate of change of virus concentration *within* a cell (note that, as with

interferon, the rate of change of the virus concentration *in the extracellular matrix* is given by a separate equation, Equation (11)):

$$\frac{dV}{dt} = \frac{k_{71}H * V}{1 + k_{72}\text{IFN}_e} - k_{73}V \quad (9)$$

The virus replicates more effectively in a healthy cell, so the increase in intracellular viral concentration is directly proportional to  $H$ , but the cell's antiviral measures, represented here by the proxy of  $\text{IFN}_e$ , can slow its progress.

### 2.3 Mathematical model of the release and diffusion of virions and interferon

In the model, virions ( $V_e$ ) and interferon molecules released from cells ( $\text{IFN}_e$ ) move through the extracellular matrix, and thus between cells, via the physical process of diffusion ([1], p. 9). Cells in any state but the death state release interferons, while only cells in the virus-releasing state release virions. In the software implementation, at each time step, eligible cells release interferons (virions) at their external boundaries at rates proportional to the ratio between interferon (virus) concentration within the cell and the cell volume. Then the entire extracellular interferon (virus) field is advanced one time step according to a differential equation designed to model diffusion with decay.

Equations (10) and (11) capture this two-step process for interferons and for the virions, respectively. In the original paper, they are Equations 10 and 11. The forms of the two equations are identical: the rate of change of the concentration of interferons or virions is equal to the effect of diffusion, plus interferon or virion secretion from cells, minus the effect of decay. These equations describe the change in external interferon and external virion concentrations *locally*, i.e., at a specific place in the extracellular matrix near a given cell;  $\text{IFN}$ ,  $V$  and  $\text{Volume}$  refer to the interferon and virion concentration within and the volume of that cell, respectively, while  $\text{IFN}_e$  and  $V_e$  refer to extracellular interferon and virion concentrations at that location.

$$\frac{\delta\text{IFN}_e}{\delta t} = D_{\text{IFN}_e} \nabla^2 \text{IFN}_e + k_{21} \frac{\text{IFN}}{\text{Volume}} - \tau_2 \text{IFN}_e \quad (10)$$

$$\frac{\delta V_e}{\delta t} = D_V \nabla^2 V_e + k_{73} \frac{V}{\text{Volume}} - c V_e \quad (11)$$

The contribution of diffusion is equal to the square of the steepness, or gradient, of the concentration field times a constant (e.g.,  $D_{\text{IFN}_e} \nabla^2 \text{IFN}_e$ , in the case of interferons;  $D_{\text{IFN}_e}$  is the diffusion constant for interferons, and  $\nabla^2 \text{IFN}_e$  is the squared gradient of the interferon field). In plain language, the more steeply the concentration of the diffusant varies over space (the gradient) and the more the diffusant tends to diffuse (the diffusion constant), the more the concentration will even out from timestep to timestep.

As mentioned above, the concentration secreted at an eligible cell's boundary is equal to the ratio between the concentration within the cell and the cell volume times a constant (e.g.,  $k_{21} \frac{\text{IFN}}{\text{Volume}}$ ;  $k_{21}$  is the secretion constant for interferons and **IFN** and **Volume** denote the interferon concentration within and the volume of a given cell). The more saturated a cell is with interferon or with virus, the more interferons or virions the cell will release (if it is in the right state to do so).

Finally, the decay process is represented as the subtraction of the product of the concentration times a constant (e.g.,  $\tau_2 \text{IFN}_e$ ;  $\tau_2$  is the interferon decay constant). So, the bigger the concentration of a diffusant at a particular location, the more that concentration will be decreased in the next moment in time.

## 2.4 Implementation with CompuCell3d

Both the original model and our replication were implemented with the modeling software CompuCell3D (CC3D). The model code is written in Python and CompuCell3D Markup Language (built on XML). Both the original code and our modified version can be downloaded from GitHub. The repository for the original code is located at [https://github.com/ImmuneSystems-Lab/Multicellular\\_Spatial\\_Model\\_of\\_RNA\\_Virus\\_Replication](https://github.com/ImmuneSystems-Lab/Multicellular_Spatial_Model_of_RNA_Virus_Replication) and the modified code can be found at <https://github.com/a-amme/infection-model-project>.

Briefly, CC3D works according to the Metropolis-Hastings algorithm, which assigns a “cost” to every possible configuration of model components and regulates changes to the configuration so that situations with higher costs are less likely to occur than those with lower costs. The cost function can be customized, and customizing the cost function is an important part of implementing a model. CC3D also supports simulated chemical fields chemical fields (e.g., this model’s **IFN<sub>e</sub>**) and the simulation of processes governed by ordinary differential equations, including chemical reactions and diffusion. For an overview of its capabilities, consult [2] or visit the project’s website

at <https://compuCell3d.org/>.

### 3 Original results

In the original paper, the authors reported the results of a “sanity check” with the model, a study of model behavior under more typical conditions, and an investigation of factors which could stop viral spread. Here, we replicate the “sanity check,” the test of the model under more realistic conditions, and the results of pre-stimulation with interferons. To aid the reader in comparison of original and reproduced results, we offer the following reproductions and descriptions of the relevant figures from [1].

To ensure that the model worked as expected, the authors averaged data from 20 runs of the model with a high multiplicity of infection (MOI) of 5, which, as they note, corresponds to the infection of all cells with one virion each (see [1], p.14). They observe that all of the cells ultimately die, though not at the same speed, which is to be expected given that the cells in the model make state transitions stochastically. They also observe IFN secretion to peak and then decline shortly after infection ([1] pp.13-5). The original paper’s Figure 2 displays data from these simulations; here, the original figure is reproduced as Figure 2.

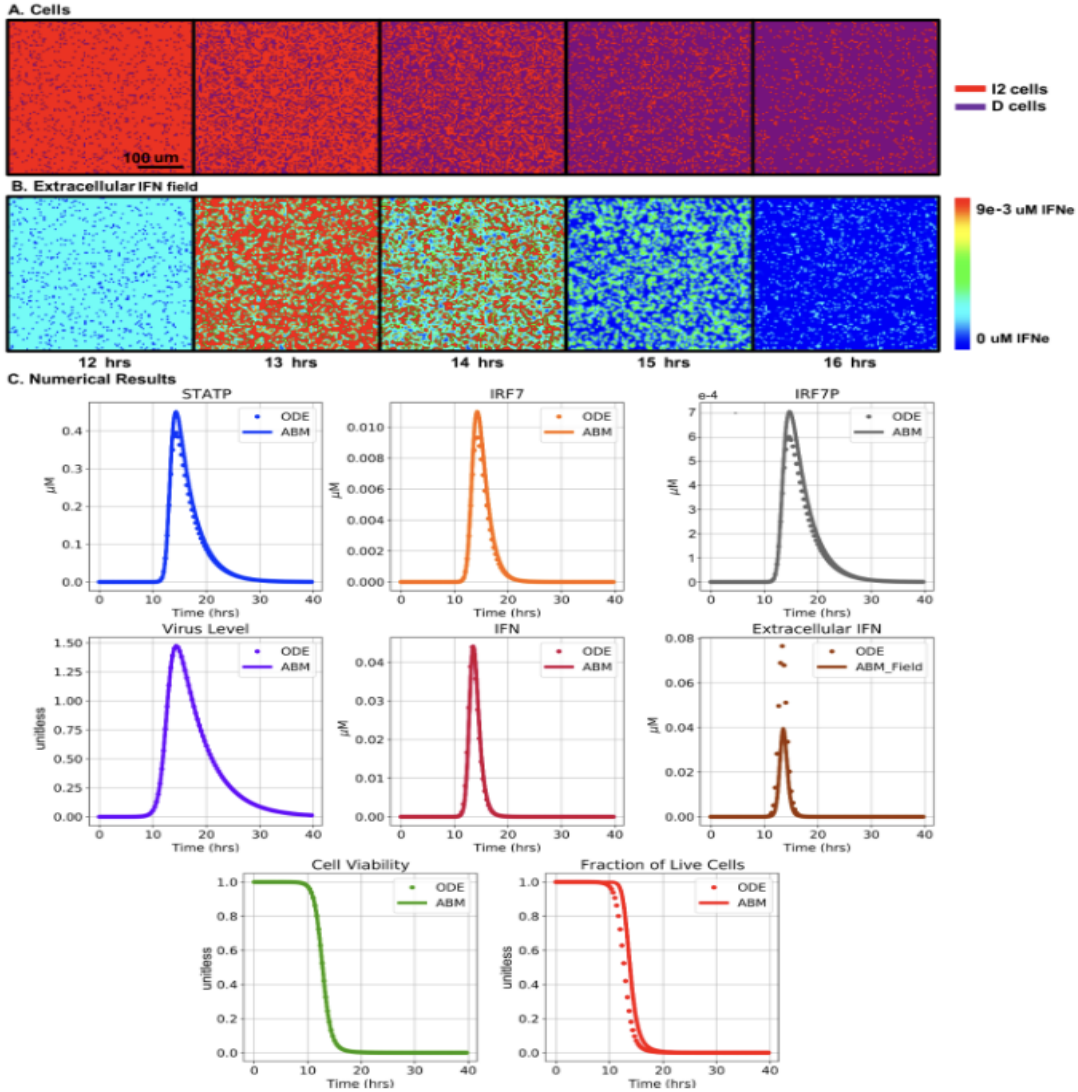


Figure 2: Screenshots and model variables from high-MOI trials reported in the original paper as Figure 2 ([1], see p. 14). A: Over 16 simulated hours, all cells progress stochastically through the infection stages to I2 (red) and then, eventually, to the death state (purple). B: Interferon release peaks after about 13 simulated hours, then declines as cells die. C: Plots of model variables (solid lines) vs. values from a purely mathematical implementation of the model (dotted lines) over 40 simulated hours. The values from the model closely track those from the purely mathematical implementation, though spikes are more intense, especially in the case of Extracellular IFN, and cells die more quickly in the mathematical implementation than in the model.

Viral infections in epithelial tissue typically spread outward from a small number of initially-infected cells. Wanting to test whether the model could capture this behavior, the researchers performed plaque growth assays by initiating the simulation with a single infected cell at the center of the cell field; they did, indeed, observe an outwardly-growing plaque of dead cells (see Figure 3, which is a reproduction of Figure 3 from [1], p. 16).

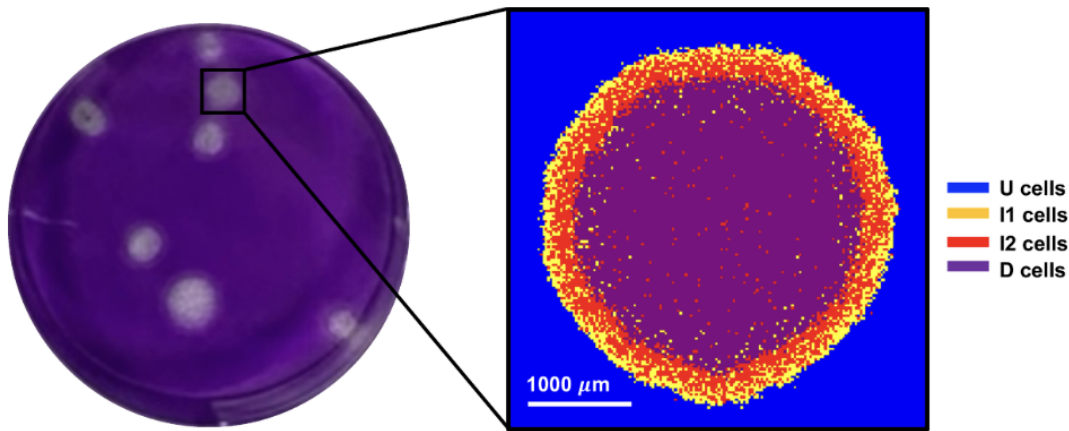


Figure 3: A screenshot from a plaque assay performed on the model juxtaposed with an image of plaques produced *in vitro*. These images appeared in the original paper as Figure 3 ([1], see p. 16).

After confirming that the model could produce plaques, the researchers compared the model's dynamics with data on two strains of influenza and studied the relationships between model variables and observed behavior. Figure 4 depicts the results of these tests, which appeared in the original paper as Figure 4.

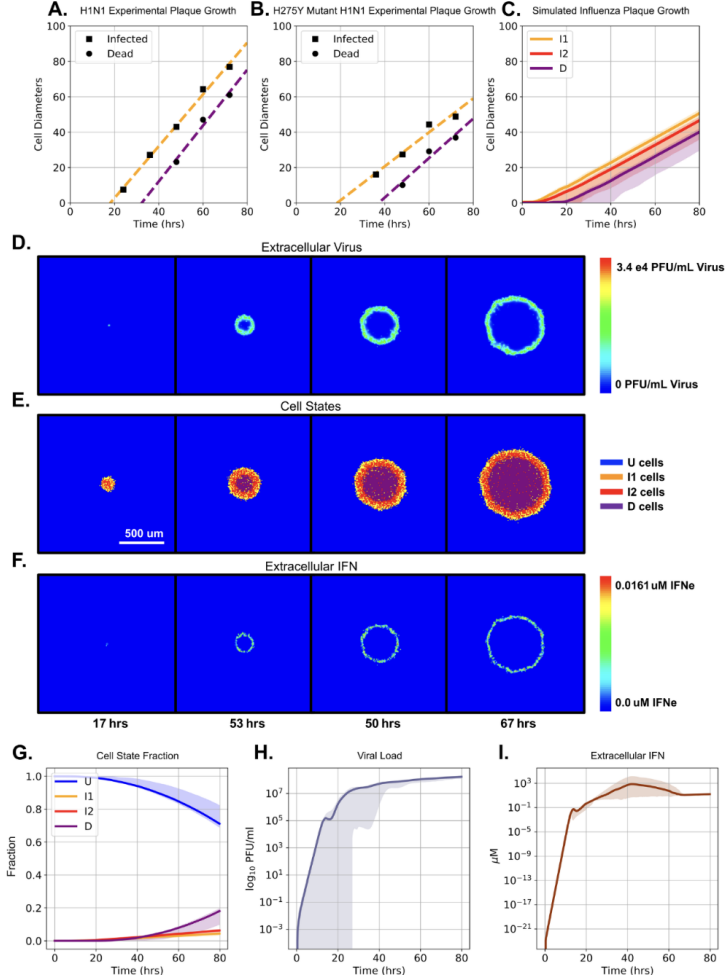


Figure 4: A study of viral plaque growth in the model reported in the original paper as Figure 4 ([1], see p. 18). Results are averages across 20 simulations. A, B, C: Linear growth in viral plaque size as a function of time in experiments with H1N1 (A), experiments with H275Y mutant H1N1 (B), and the model (C). Model results are qualitatively similar to these data, though growth is slower in the model. D, E, F: visualizations of viral plaque growth with focus on extracellular virion concentrations, or  $V_e$  (D), cell state (E), and extracellular interferon concentration  $IFN_e$ . G, H, I: visual summaries of plaque growth, including plots of the proportion of cells in each of the four states (G), a plot of the viral load in the tissue across time (H), and a plot of the extracellular IFN concentration  $IFN_e$ . In these plots, the line is the mean value, while the shaded region is the area between the minimum and maximum values.

The original paper included several studies to the end of exploring potential targets for the slow-

ing of plaque growth. We are particularly interested in the therapeutic potential of pre-treatment with interferons, so we chose to replicate the relevant simulations. The original paper reports that in simulations where  $\text{IFN}_e$  was set high at initialization, a single cell was placed in the infected state, and then  $\text{IFN}_e$  was lowered, the plaque stopped growing long before it could consume the simulated cell culture. The original Figure 7 showed these results; here we reproduce that figure in Figure 5.

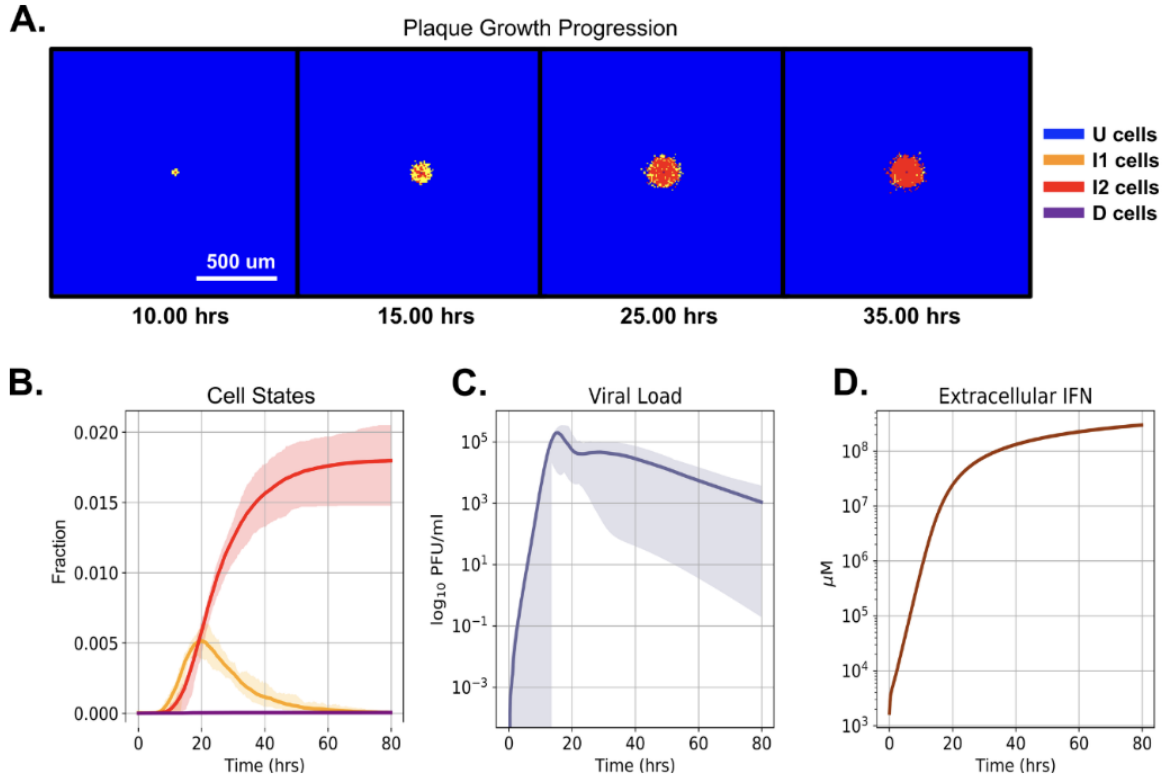


Figure 5: Average results of 20 simulations in which uninfected cells were pre-treated with extracellular IFN. A: the viral plaque grows very slowly, then ceases to grow at around 25 simulated hours post-infection. B: the proportions of cells in the different infected states throughout the simulation. Note that there are very few dead cells. C: Viral load increases quickly until about 15 simulated hours after infection, following which it begins to decrease. D: The cells mount a vigorous IFN response. Note that in B, C, and D, the line represents the average value observed across the 20 simulations, while the shaded area is the region between the minimum and maximum values. In the original paper, these images appear in Figure 7 ([1], see p.25).

## 4 Changes and optimizations

We have produced code that is more cleanly written and runs faster than the original. To improve code readability, we combined `for` loops where possible. We also deactivated data file outputs, which improved the speed of execution markedly.

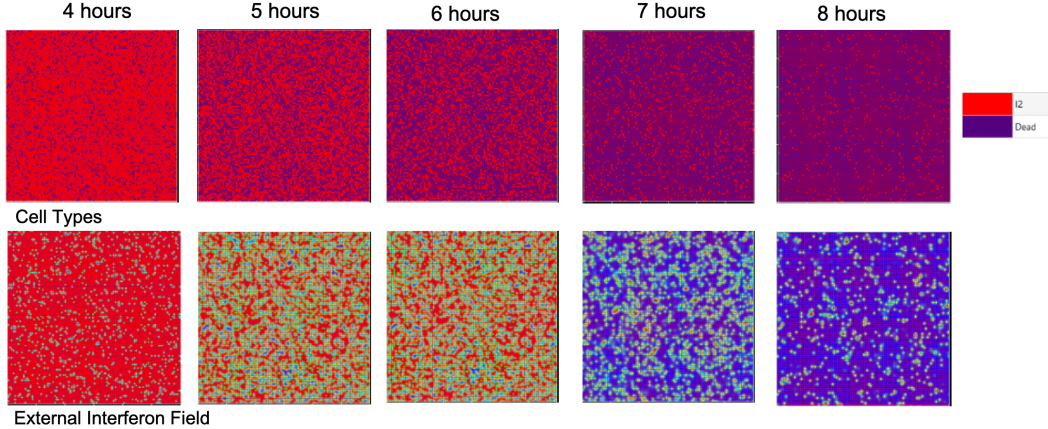
Finally, we added sliders for eight model or simulation parameters: interferon and virus diffusion constants,  $D_{IFN_e}$  and  $D_{V_e}$ , interferon and virus decay rates,  $\tau_2$  and  $c$ , the rate of cell health loss,  $k_{61}$ , the rate of STAT activation,  $k_{31}$ , RIG-I activity (which is set to zero by default),  $k_{11}$ , and MOI.

## 5 Replication results

We were able to qualitatively replicate all of our targeted figures, namely original Figures 2, 3, 4, and 7.

Our Figure 6 corresponds to the original 2; it shows the behavior of the high-MOI simulations. As in the original paper, we found that all of the cells progress stochastically through the health states to death. The plots of the parameter values throughout the simulation look identitcal to those from the original paper. However, the virus appears to have progressed twice as fast in our replication than in the original model. The cause is not clear upon inspection of the code, as the two simulations use the same equations and the same parameter values.

Our Figure 7 depicts the results of our attempt to replicate the plaque assay experiments from the original paper, reported there in Figures 3 and 4 [1]. The plaque growth we observed looks quite similar to what was reported in the paper. The plots of the proportions of cell types present in the simulation over time, which comprise the bottom panel of Figure 7, also look qualitatively similar to the target results, but it is clear from our replicated plot that the infection progressed more quickly in our simulations than in the simulations reported in the original paper. Our plots of the average extracellular virus and interferon concentrations, which appear roughly linear, do, in fact, replicate the original result, as the authors of the original paper used a logarithmic scale for the concetrations; linear growth growth on a linear scale is logarithmic growth on a logarithmic scale.



(a) The progress of a simulated viral plaque assay experiment. The top row of images shows cells in the I2 virus-releasing state (red) vs. the dead state (purple). The bottom row shows the concentration of extracellular interferons.

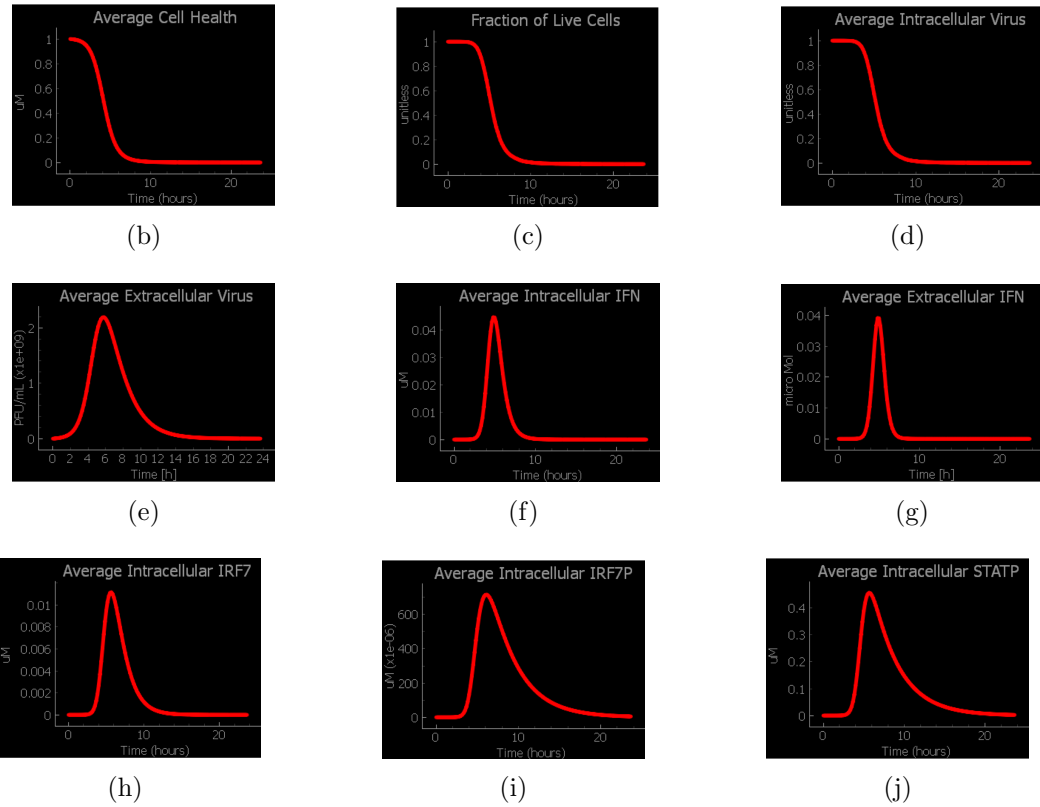


Figure 6: The products of our successful attempt to replicate Figure 2 from [1]. The plots give the values of model variables, including cell health and concentrations of the simulated chemicals, throughout the simulated experiment depicted in the top panel.

## Time course of viral spread, default parameters

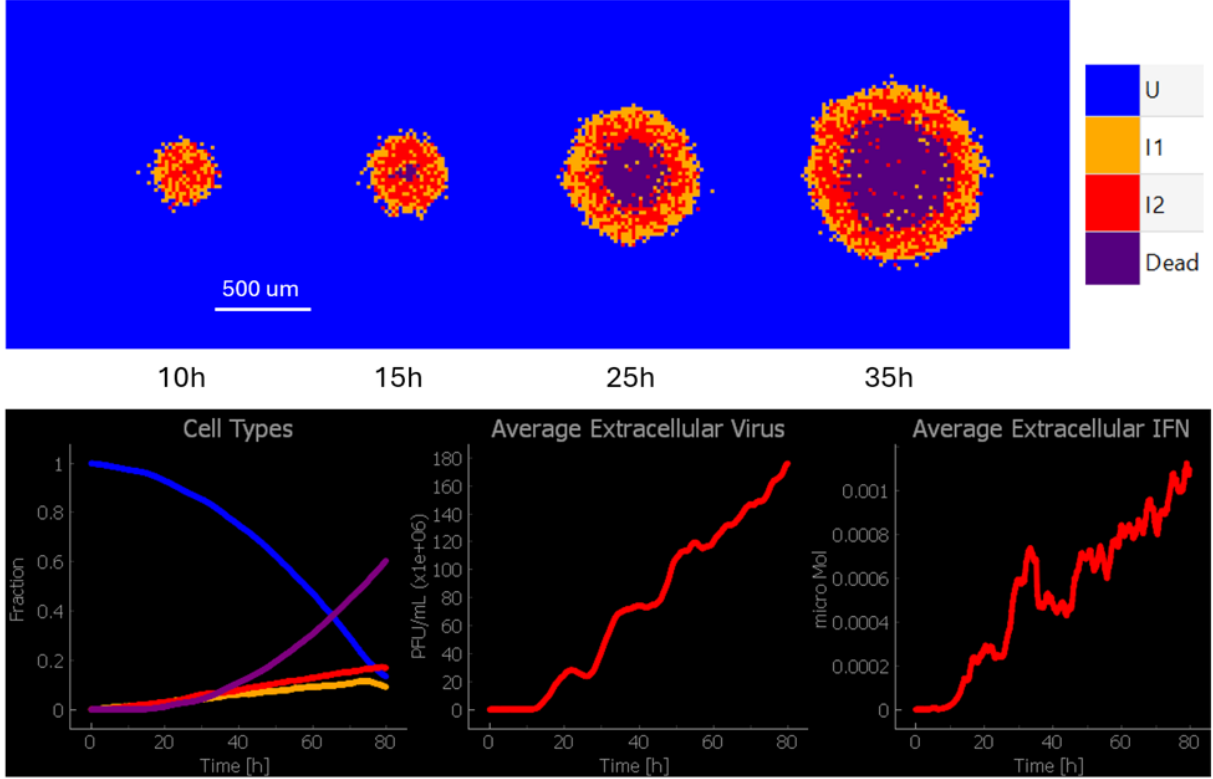


Figure 7: Our successful replication of Figure 3 and portions of Figure 4 from [1] (pp. 16 and 18, respectively). Top: Replicating the original paper’s Figure 3, we simulated viral plaque assay methods using our model and observed plaque growth as expected. Bottom: Plots of the proportions of the different cell types present (left), average extracellular virion concentration (middle), and average extracellular interferon concentration (right) over the course of the simulation were qualitatively similar to the originals; note that our  $V_e$  and  $\text{IFN}_e$  plots have linear scaling, while the originals use logarithmically scaled data.

Our ultimate goal was to replicate the original paper’s result demonstrating that pre-treatment of the simulated cell culture with interferons slows plaque growth to a stop. We succeeded in making a qualitative replication this finding; images and plots from our simulation can be found in Figure 8. Pre-treatment of our simulated cell culture with interferon resulted in the cessation of plaque growth by around 35 simulated hours post-infection. Plaques grew bigger in our replication than they did in the original work, and we observed more cell death than we had expected based on the original findings. Our plot of average extracellular virus concentration appears to differ from the original figure, though in both plots, the concentration peaks near  $10^6$  PFU/mL at around 20 simulated

hours. Oddly, the interferon response we observed was orders of magnitude less intense than was reported in the original paper, a fact which may account for the faster and wider viral spread in our simulations. In the original work, the maximum average extracellular IFN concentration observed in the IFN-pre-treatment simulations exceeded that seen in the untreated plaque assay experimentations by about ten orders of magnitude. In our replications, the two values differed by about eight orders of magnitude.

### Time course of viral spread with pre-exposure to IFN

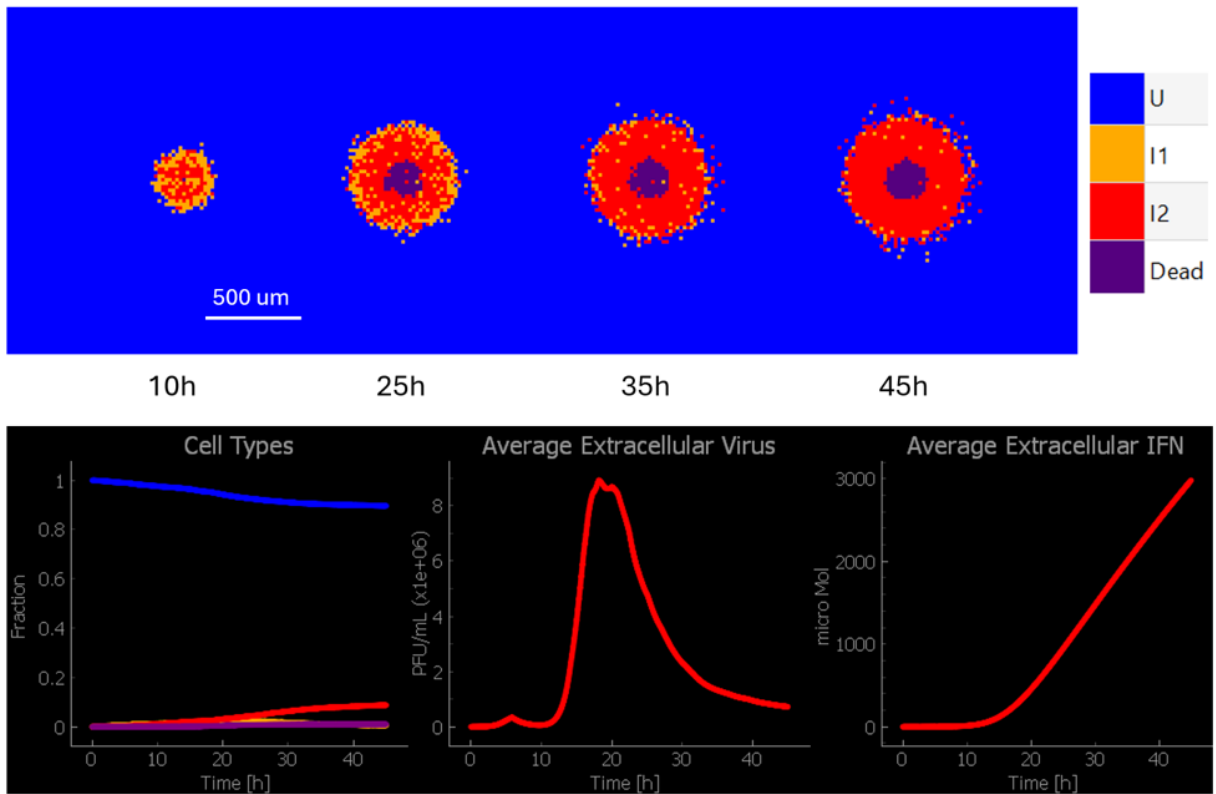


Figure 8: The results of our attempts to replicate the simulations with interferon pre-treatment reported in the original paper in Figure 7 (see [1], p.25). Top: Pre-treatment with IFN causes plaque growth to slow to a stop, replicating the result, although our plaque grows more quickly and ultimately consumes a larger portion of the simulated cell culture. Bottom: Plots of the proportions of the different cell types present (left), average extracellular virion concentration (middle), and average extracellular interferon concentration (right) over the course of the simulation.

## References

- [1] Joshua O. Aponte-Serrano et al. “Multicellular spatial model of RNA virus replication and interferon responses reveals factors controlling plaque growth dynamics”. In: *PLoS Computational Biology* 17.10 (2021), e1008874. DOI: [10.1371/journal.pcbi.1008874](https://doi.org/10.1371/journal.pcbi.1008874).
- [2] Maciej H. Swat et al. “Multi-scale modeling of tissues using CompuCell3D”. In: *Methods of Cell Biology* 110 (2013), pp. 325–66. DOI: [10.1016/B978-0-12-388403-9.00013-8](https://doi.org/10.1016/B978-0-12-388403-9.00013-8).
- [3] A. Baer and K. Kehn-Hall. “Viral concentration determination through plaque assays using traditional and novel overlay systems”. In: *Journal of Visualized Experiments* 93 (2014), p. 52065. DOI: [10.3791/52065](https://doi.org/10.3791/52065).
- [4] B. Alberts et al. *Molecular Biology of the Cell, Fourth Edition*. W. W. Norton & Company, 2002.
- [5] A. M. Kell and M. Gale. “RIG-I in RNA virus recognition”. In: *Virology* 479 (2015), pp. 110–21. DOI: [10.1016/j.virol.2015.02.017](https://doi.org/10.1016/j.virol.2015.02.017).
- [6] K. A. Fitzgerald and J. C. Kagan. “Toll-like receptors and the control of immunity”. In: *Cell* 180.6 (2020), pp. 1044–66. DOI: [10.1016/j.cell.2020.02.041](https://doi.org/10.1016/j.cell.2020.02.041).
- [7] M. Fribourg et al. “Model of Influenza A virus infection: dynamics of viral antagonism and innate immune response”. In: *Journal of Theoretical Biology* 351 (2014), pp. 47–57. DOI: [10.1016/j.jtbi.2014.02.029](https://doi.org/10.1016/j.jtbi.2014.02.029).
- [8] A. F. Wilks. “Two putative protein-tyrosine kinases identified by application of the polymerase chain reaction”. In: *Proceedings of the National Academy of the Sciences* 86.5 (1989), pp. 1603–7. DOI: [10.1073/pnas.86.5.1603](https://doi.org/10.1073/pnas.86.5.1603).
- [9] T. Kisseeleva et al. “Signaling through the JAK/STAT pathway, recent advances and future challenges”. In: *Gene* 285.1-2 (2002), pp. 1–24. DOI: [10.1016/s0378-1119\(02\)00398-0](https://doi.org/10.1016/s0378-1119(02)00398-0).
- [10] A. M. Smith and A. S. Perelson. “Influenza A virus infection kinetics: Quantitative data and models”. In: *Wiley Interdisciplinary Reviews Systems Biology and Medicine* 3.4 (2011), pp. 429–45. DOI: [10.1002/wsbm.129-8](https://doi.org/10.1002/wsbm.129-8).

- [11] J. J. A. Weaver and J. E. Shoemaker. “Mathematical modeling of RNA virus sensing pathways reveals paracrine signaling as the primary factor regulating excessive cytokine production”. In: *Processes* 8.6 (2020), p. 719. DOI: [10.3390/pr8060719](https://doi.org/10.3390/pr8060719).
- [12] A. M. Smith and A. S. Perelson. “Influenza A virus infection kinetics: Quantitative data and models”. In: *Wiley Interdisciplinary Reviews Systems Biology and Medicine* 3.4 (2011), pp. 429–45. DOI: [10.1002/wsbm.129-8](https://doi.org/10.1002/wsbm.129-8).
- [13] L. V. Sharova et al. “Database for mRNA half-life of 19977 genes obtained by DNA microarray analysis of pluripotent and differentiating mouse embryonic stem cells”. In: *DNA Research* 16.1 (2009), pp. 45–58. DOI: [10.1093/dnare/dsn030](https://doi.org/10.1093/dnare/dsn030).
- [14] A. Prakash and D. E. Levy. “Regulation of IRF7 through cell type-specific protein stability”. In: *Biochemical and Biophysical Research Communications* 342.1 (2006), pp. 50–6. DOI: [10.1016/j.bbrc.2006.01.122](https://doi.org/10.1016/j.bbrc.2006.01.122).

## A Table of Constants

Parameter	Value	Units	Process	Source
$k_{11}$	0.0	$\mu\text{m hr}^{-1}$	RIG-I sensing	[11]
$k_{12}$	9.746	$\text{h}^{-1}$	TLR sensing	[11]
$k_{13}$	12.511	[unitless]	TLR sensing	[11]
$k_{14}$	13.562	$\text{h}^{-1}$	IFN production via IRF7P	[11]
$k_{21}$	10.385	$\text{h}^{-1}$	IFN export rate	[11]
$\tau_2$	3.481	$\text{h}^{-1}$	IFN <sub>e</sub> decay	[11]
$k_{31}$	45.922	$\mu\text{m hr}^{-1}$	JAK/STAT activation from IFN <sub>e</sub>	[11]
$k_{32}$	5.464	$\mu\text{m}$	JAK/STAT activation from IFN <sub>e</sub>	[11]
$k_{33}$	0.068	[unitless]	JAK/STAT activation from IFN <sub>e</sub>	[11]
$t_3$	0.3	$\text{h}^{-1}$	STATP dephosphorylation	[12]
$k_{41}$	0.115	$\text{h}^{-1}$	IRF7 induction via STATP	[11]
$t_{42}$	1.053	$\text{h}^{-1}$	IRF7 induction via STATP	[11]
$t_4$	0.75	$\text{h}^{-1}$	IRF7 decay	[11], [13]
$k_{51}$	0.202	$\text{h}^{-1}$	IRF7 phosphorylation	[11]
$t_5$	0.3	$\text{h}^{-1}$	IRF7P dephosphorylation	[14]
$k_{61}$	0.635	$\text{h}^{-1}$	Loss of cell viability	[11]
$k_{71}$	1.537	$\text{h}^{-1}$	Viral production	[11]
$k_{72}$	47.883	$\mu\text{m}^{-1}$	Saturation of viral production	[11]
$k_{73}$	0.197	$\text{h}^{-1}$	Nonspecific viral clearance in extracellular environment	[11]

$n$	3	[unitless]	Kinetic order term	[11]
$\beta$	$2.4 \times 10^4$	PFU/mL days <sup>-1</sup>	Viral infectivity	[2]
$c$	13	days <sup>-1</sup>	Viral decay	[2]
$k$	4	days <sup>-1</sup>	Eclipse phase delay	[2]
$D_{V_e}$	54.0	$\mu\text{m}^2 \text{ s}^{-1}$	Viral diffusion constant	[1]
$D_{IFN_e}$	54.0	$\mu\text{m}^2 \text{ s}^{-1}$	IFN <sub>e</sub> diffusion constant	[1]
Lattice	3	$\mu\text{m}$	Width of lattice squares	[1]
MCS	10	minutes	Monte Carlo step	[1]
Cell size	4.5	$\mu\text{m}$	Cell's radius	[1]

Table 1: All constants for the model along with their sources. Reproduced from [1], p. 11-2.